Published in final edited form as:
Bone. 2023 August ; 173: 116808. doi:10.1016/j.bone.2023.116808.

Assessing cortical bone porosity with MRI in an animal model of chronic kidney disease

Christopher L. Newman[a,*], **Rachel K. Surowiec**[b], **Elizabeth A. Swallow**[c], **Corinne E. Metzger**[d], **Jieun Kim**[d], **Andrew A. Tomaschke**[b], **Neal X. Chen**[f], **Matthew R. Allen**[b,e,f], **Joseph M. Wallace**[b], **Sharon M. Moe**[f], **Yu-Chien Wu**[a], **Paul J. Niziolek**[a]

[a]Department of Radiology and Imaging Sciences, Indiana University School of Medicine, Indianapolis, IN, United States of America

[b]Department of Biomedical Engineering, Indiana University-Purdue University, Indianapolis, Indianapolis, IN, United States of America

[c]The University of the South, Sewanee, TN, United States of America

[d]Wu Tsai Neurosciences Institute, Stanford University, Stanford, CA, United States of America

[e]Department of Anatomy, Cell Biology, and Physiology, Indiana University School of Medicine, Indianapolis, IN, United States of America

[f]Division of Nephrology, Department of Medicine, Indiana University School of Medicine, Indianapolis, IN, United States of America

Abstract

Chronic kidney disease (CKD) is characterized by secondary hyperparathyroidism and an increased risk of hip fractures predominantly related to cortical porosity. Unfortunately, bone

*Corresponding author at: Department of Radiology and Imaging Sciences, Indiana University School of Medicine, 705 Riley Hospital Drive, Room 1053, Indianapolis, IN 46202, United States of America., chrnewma@iu.edu (C.L. Newman).

Declaration of competing interest
None.

CRediT authorship contribution statement
Christopher L. Newman: Conceptualization, Data curation, Formal analysis, Funding acquisition, Investigation, Methodology, Project administration, Resources, Software, Supervision, Validation, Visualization, Writing – original draft, Writing – review & editing. **Rachel K. Surowiec:** Data curation, Formal analysis, Investigation, Methodology, Resources, Software, Validation, Visualization, Writing – original draft, Writing – review & editing. **Elizabeth A. Swallow:** Data curation, Formal analysis, Investigation, Methodology, Resources, Software, Validation, Visualization, Writing – original draft, Writing – review & editing. **Corinne E. Metzger:** Data curation, Formal analysis, Investigation, Methodology, Resources, Software, Validation, Visualization, Writing – original draft, Writing – review & editing. **Jieun Kim:** Data curation, Formal analysis, Investigation, Methodology, Resources, Software, Validation, Writing – review & editing, Writing – original draft. **Andrew A. Tomaschke:** Data curation, Formal analysis, Investigation, Methodology, Resources, Software, Visualization, Validation, Writing – original draft, Writing – review & editing. **Neal X. Chen:** Conceptualization, Data curation, Investigation, Methodology, Project administration, Resources, Software, Supervision, Writing – original draft, Writing – review & editing. **Matthew R. Allen:** Conceptualization, Data curation, Formal analysis, Funding acquisition, Investigation, Methodology, Project administration, Resources, Supervision, Writing – original draft, Writing – review & editing. **Joseph M. Wallace:** Conceptualization, Data curation, Formal analysis, Investigation, Methodology, Project administration, Resources, Supervision, Writing – original draft, Writing – review & editing. **Sharon M. Moe:** Conceptualization, Data curation, Formal analysis, Investigation, Methodology, Project administration, Resources, Supervision, Writing – original draft, Writing – review & editing. **Yu-Chien Wu:** Conceptualization, Data curation, Formal analysis, Investigation, Methodology, Project administration, Resources, Supervision, Writing – original draft, Writing – review & editing. **Paul J. Niziolek:** Conceptualization, Data curation, Formal analysis, Funding acquisition, Investigation, Methodology, Project administration, Resources, Software, Supervision, Validation, Visualization, Writing – original draft, Writing – review & editing.

mineral density measurements and high-resolution peripheral computed tomography (HR-pQCT) imaging have shortcomings that limit their utility in these patients. Ultrashort echo time magnetic resonance imaging (UTE-MRI) has the potential to overcome these limitations by providing an alternative assessment of cortical porosity. The goal of the current study was to determine if UTE-MRI could detect changes in porosity in an established rat model of CKD.

Cy/+ rats (n = 11), an established animal model of CKD-MBD, and their normal littermates (n = 12) were imaged using microcomputed tomography (microCT) and UTE-MRI at 30 and 35 weeks of age (which approximates late-stage kidney disease in humans). Images were obtained at the distal tibia and the proximal femur. Cortical porosity was assessed using the percent porosity (Pore%) calculated from microCT imaging and the porosity index (PI) calculated from UTE-MRI. Correlations between Pore% and PI were also calculated.

Cy/+ rats had higher Pore% than normal rats at both skeletal sites at 35 weeks (tibia = 7.13 % +/− 5.59 % *vs.* 0.51 % +/− 0.09 %, femur = 19.99 % +/− 7.72 % *vs.* 2.72 % +/− 0.32 %). They also had greater PI at the distal tibia at 30 weeks of age (0.47 +/− 0.06 *vs.* 0.40 +/− 0.08). However, Pore% and PI were only correlated in the proximal femur at 35 weeks of age (ρ = 0.929, Spearman).

These microCT results are consistent with prior studies in this animal model utilizing microCT imaging. The UTE-MRI results were inconsistent, resulting in variable correlations with microCT imaging, which may be related to suboptimal bound and pore water discrimination at higher magnetic field strengths. Nevertheless, UTE-MRI may still provide an additional clinical tool to assess fracture risk without using ionizing radiation in CKD patients.

Keywords

Chronic kidney disease; MRI; UTE; Porosity index; microCT

1. Introduction

Disturbances in bone and mineral metabolism are a hallmark of chronic kidney disease—mineral and bone disorder (CKD-MBD) [1,2]. Along with hyperphosphatemia, secondary hyperparathyroidism, and vascular calcifications, patients exhibit a high risk of hip fractures [3–9]. The metabolic complexity associated with CKD has led to great challenges in understanding its various skeletal manifestations [10], which has led to difficulty predicting fractures in these patients.

Though bone mineral density (BMD) can predict fracture in CKD patients and is recommended for screening by clinical practice guidelines [11,12], it likely underestimates true fracture risk since studies have produced inconsistent results [13–16]. In addition, the predictive value of BMD diminishes with worsening hyperparathyroidism [16]. One potential explanation for these inconsistencies is the fact that cortical bone is preferentially impacted in these patients, and its loss cannot be differentiated from trabecular bone loss by standard areal BMD measurements [17]. The formation and expansion of cortical pores predominate in CKD and are correlated with impaired mechanical properties [17].

Because of its ability to differentiate between cortical and trabecular bone, high-resolution peripheral quantitative computed tomography imaging (HR-pQCT) has been shown to have greater predictive utility for patients with CKD [9]. Similar results have been demonstrated in animal models using microcomputed tomography (microCT) imaging [18]. Unfortunately, HR-pQCT is limited to peripheral sites (radius and tibia) because the size of the imaging bore precludes evaluation of the hip. This, along with other barriers to its widespread adoption [19], has limited the use of HR-pQCT to research studies.

Advances in ultrashort echo time magnetic resonance (UTE-MR) imaging techniques have been employed to obtain signal from skeletal tissue that is not normally detectable using standard clinical MRI sequences [20,21]. With the subsequent advent of biexponential analysis, the water molecules freely flowing within pores can now be distinguished from the water molecules bound to the bone matrix [22]. Hence, these newer techniques provide additional biochemical information inaccessible to the morphological assessment provided by conventional bone imaging [23].

Recent UTE-MRI studies have demonstrated that an abbreviated version of the biexponential analysis, known as the porosity index (PI), can still distinguish bound water from free water in bone [24,25]. In addition, calculation of the PI requires measuring signal decay at only two echo times and has the potential to significantly reduce overall scan time. PI is correlated with cortical porosity derived from high-resolution CT imaging and inversely correlated with mechanical properties [26–29]. The goal of the current study was to determine the ability of the PI derived from UTE-MRI to detect changes in cortical porosity in animals with progressively worsening CKD bone disease. Three specific questions were addressed. First, can the PI detect changes in the distal tibia observed with *in vivo* microCT imaging? Second, can the PI detect changes in cortical porosity in the proximal femur observed with *ex vivo* microCT imaging? Third, is there a correlation between the PI and bone strength in the proximal femur? These questions were addressed by testing the hypothesis that the PI would detect changes in cortical bone porosity observed with microCT imaging across multiple bone sites and would correlate with femoral neck mechanical properties.

2. Materials and methods

2.1. Animals and experimental design

Male Cy/+ rats ($n = 11$) and their normal male littermates ($n = 12$) were utilized. Cy/+ rats develop gradual disturbances in mineral metabolism and provide a model of progressive hyperphosphatemia, hyperparathyroidism, and skeletal abnormalities [30–33]. Skeletal abnormalities are normally present by 28–30 weeks and progress to severe phenotypic changes by 33–35 weeks, including the development of severe cortical porosity [18]. On the contrary, female Cy/+ rats have a much less predictable pattern of disease progression [34]. Because of this heterogeneity, male Cy/+ rats were employed in the current study. Rats were bred in-house and phenotyped into CKD or normal groups by plasma blood urea nitrogen (BUN) measured at 10 weeks of age by colorimetric assay (BioAssay Systems, Hayward, CA, USA). Rats were singly housed throughout the duration of the study in a facility with 12-hour light/dark cycles. At 24 weeks of age, all rats were switched to a

purified casein-based diet with 0.7 % phosphorus and 0.7 % calcium (Envigo, Madison, WI, USA) for the remainder of the study protocol. Food and water were provided *ad libitum* throughout the entire study.

Rats were evaluated with *in vivo* imaging at 30 and 35 weeks of age (Fig. 1), which corresponds to approximately 10–20 % of normal kidney function. At 35 weeks, animals were anesthetized and euthanized with carbon dioxide prior to tissue collection. Four CKD animals died between 33 and 35 weeks of age due to terminal uremia prior to repeat imaging and were excluded from imaging analysis at 35 weeks of age. One animal requiring early euthanasia was imaged at 33 weeks of age and included in the analysis at 35 weeks given its advanced disease. The right tibiae and femora were harvested, wrapped in saline soaked gauze, and stored at −20 °C for *ex vivo* imaging and mechanical testing. These procedures were conducted with the approval of the Indiana University School of Medicine Institutional Animal Care and Use Committee.

2.2. UTE-MR imaging

At 30 and 35 weeks of age, the right distal tibiae and right proximal femora of the animals in each group were analyzed with *in vivo* UTE-MR imaging. Rats were anesthetized *via* inhaled vaporized isoflurane and then placed supine in the bed of the scanner with the right lower extremity secured in the field of view. Using a 9.4 T small animal MRI scanner (Bruker BioSpec 94/30 USR) with a rat body surface array coil, a 3D UTE sequence with a voxel size of 234 μm was performed using dual echoes (TE1 = 0.007 ms, TE2 = 2 ms) with the following scan parameters: 128 × 128 acquisition matrix, flip angle of 4 degrees, repetition time of 10 s, and respiratory gating (resulting in a total scan time of 42 min per site). The proximal femora and distal tibiae were scanned separately with the body coil centered over each anatomic site. The PI was calculated for each anatomic site. The image obtained from the first echo reflects the signal arising from the total bone water within the region of interest (extremely short T2* relaxation time), whereas the image from the second echo reflects signal arising from the water freely flowing within the bone pores (longer T2* relaxation time) [23,24]. The signal intensity from each pixel in the second echo was divided by the signal intensity from each pixel in the first echo to provide a porosity index value for each pixel. These values were averaged over a 1 mm cortical bone volume of interest (VOI). At the distal tibia, a VOI was used 1 mm proximal to the tibiofibular junction (Fig. 2). Because the femoral neck cortex is thin and has a low signal-to-noise ratio [35], the proximal femoral diaphysis was analyzed using a VOI positioned 1 mm distal to the lesser trochanter (Fig. 2).

2.3. microCT imaging

At 30 weeks of age, the right distal tibiae were imaged using *in vivo* microCT imaging (Bruker Skyscan 1176). Rats were anesthetized *via* inhaled vaporized isoflurane and then placed supine in the bed of the scanner with the right leg secured in the field of view. Scans were completed with a 1.0 mm aluminum filter, 9 μm voxel size, and a 0.5 rotation step without frame averaging. Each *in vivo* scan took approximately 11 min. Four normal animals were scanned at 30 weeks of age to confirm that the cortical bone morphology of normal rats conformed to the previously established phenotype [30–33]. Because the

imaging gantry is too small to conduct *in vivo* imaging of the proximal femur, *ex vivo* imaging was required. After euthanasia, the right distal tibiae and right proximal femora were imaged using *ex vivo* microCT imaging (Bruker Skyscan 1172) with a 0.5 mm aluminum filter, 12 mm voxel size, 0.7 rotation step, and two frame averages.

Scans were reconstructed with Bruker software (NRecon) with smoothing level 2 (using a Gaussian smoothing kernel), level 8 ring artifact reduction, and 20 % beam-hardening correction. All samples were reconstructed at a dynamic image range of 0.0 to 0.09. Following reconstruction, scans were rotated to a standard orientation for each bone site (DataViewer, Bruker). Outcome parameters were assessed from manually drawn regions of interest tracing the periosteal and endosteal surfaces. Bone volume was measured including the void spaces (pores) between the periosteal and endosteal surfaces using 1 mm VOIs positioned 1 mm proximal to the tibiofibular junction and 1 mm distal to the lesser trochanter corresponding to the VOIs used for UTE-MRI (Fig. 3). Cortical bone porosity (Pore%) was defined as the percent of void space within the cortical bone region or the inverse of bone volume (1 – bone volume/total volume). The distal tibiae and proximal femora from the four CKD animals that died early were imaged with *ex vivo* microCT imaging and included in the microCT analysis at 35 weeks given their advanced stage of disease.

2.4. Mechanical testing

Fresh frozen right femora were thawed to room temperature and cut at the femoral midshaft using a rotary saw, and the remaining portions of the proximal femora were fixed in a low melting point bismuth alloy for mechanical testing. A flat compressive platen was brought into contact with the top of the femoral head and displaced downward until failure (defined as a 50 % decrease in load) at a rate of 0.025 mm/s using a electromechanical universal testing system (Test Resources 100 Series Test Instrument). Following testing, load-displacement curves for each sample were analyzed to determine the maximum strength (ultimate load). Four femora from normal animals and two femora from CKD animals were damaged during preparation and excluded from analysis. Because the two damaged bones from the CKD animals were from the seven animals that received *in vivo* UTE-MRI imaging at 35 weeks of age, only five animals were included in the correlation analysis between UTE-MRI and ultimate load. All nine CKD samples that underwent mechanical testing were included in the correlation analysis between microCT and ultimate load.

2.5. Statistical analysis

Shapiro-Wilk tests were used to assess normality within each group, and Levene's tests of equal variance were used to assess variance between groups. Outcomes among CKD animals and normal animals at 30 weeks and 35 weeks of age were analyzed using two-way ANOVA. For significant results among groups, pairwise comparisons were performed using Tukey's tests. For outcomes only evaluated at 35 weeks of age, group differences were analyzed using Welch's *t*-tests. All correlations were analyzed using Spearman's rank correlation coefficients. All analyses were performed using SPSS version 28.0.1.1 (IBM),

and p-values <0.05 were used for statistical significance. Data are presented as mean +/− standard deviation.

3. Results

3.1. microCT

At both 30 weeks of age (*in vivo*), Cy/+ rats did not have a greater Pore% than their normal littermates. However, the Pore% was higher in Cy/+ rats at 35 weeks of age (*ex vivo*) (Fig. 4a). In addition, the Pore% in animals with CKD substantially increased over the course of the study (Fig. 4a). Finally, Cy\ + rats had a higher *ex vivo* proximal femur Pore% than their normal counterparts at 35 weeks of age (Fig. 4b).

3.2. UTE-MRI

At 30 weeks of age, Cy/+ rats had a greater distal tibia PI compared to their normal counterparts (Fig. 5a). There was no difference between normal and Cy/+ groups at 35 weeks of age (Fig. 5a), nor was there a change in PI in the distal tibia in Cy/+ rats over time (Fig. 3a).

There was no difference in the proximal femur PI between Cy/+ rats and normal rats at either 30 weeks of age or 35 weeks of age (Fig. 5b), though there was a trend (ANOVA = 0.083) driven by the nonsignificantly higher mean PI in animals with CKD. As with the distal tibia, there was no increase in the proximal femur PI among Cy/+ rats over time (Fig. 5b).

3.3. Mechanics

Animals with CKD had a lower femoral neck ultimate load compared to their normal counterparts (Fig. 6). There was no significant correlation between the distal tibia PI and ultimate load or between the proximal femur PI and ultimate load in Cy/+ rats at 35 weeks of age (Fig. 7a and b). On the other hand, Pore% was negatively correlated with femoral neck mechanical properties at both sites at 35 weeks of age (Fig. 7c and d). In normal animals on the other hand, there were no significant correlations between ultimate load and distal tibia PI ($\rho = -0.299$, $p = 0.471$), proximal femur PI ($\rho = 0.587$, $p = 0.126$), distal tibia Pore% ($\rho = -0.084$, $p = 0.844$), or proximal femur Pore% ($\rho = 0.143$, $p = 0.736$) at 35 weeks of age.

3.4. UTE-MRI and microCT correlations

There was no significant correlation between the distal tibia PI and Pore% in animals with CKD at 30 (Fig. 8a) or 35 weeks of age (Fig. 8b). However, PI and Pore% were positively correlated in the proximal femur at 35 weeks of age (Fig. 8c). In normal animals on the other hand, there was no significant correlation between PI and Pore% at either the distal tibia ($\rho = -0.175$, $p = 0.586$) or the proximal femur ($\rho = -0.70$, $p = 0.828$) at 35 weeks of age.

4. Discussion

Although prior studies have examined the relationship between high resolution CT imaging and UTE-MRI [26–28], this was the first to prospectively examine their relationship in the setting of a disease characterized by substantial cortical porosity (CKD-MBD). This was accomplished by performing microCT and UTE-MRI at two different anatomic sites and at two different times throughout the course of advancing disease. This examination represents an important step for attempting to validate UTE-MR imaging in the setting of CKD because the PI may provide a useful, non-irradiating method for monitoring the progression of bone disease in these patients [36].

As with prior studies in this CKD animal model [18,37], this study demonstrated severe progressive cortical porosity with microCT imaging. In addition, these phenotypic changes were correlated with inferior mechanical properties demonstrated by femoral neck testing ($\rho = -0.983$ with the distal tibia, $\rho = -0.750$ with the proximal femur). These findings continue to highlight the role that cortical porosity plays in the bone fragility caused by CKD. Unfortunately, imaging of the hip (the most common site of fracture) is inaccessible with HR-pQCT [19]. With short scan times and the ability to evaluate the proximal femur [20], UTE-MR imaging (with derivation of the porosity index) holds promise as a method by which to monitor disease progression at the most clinically relevant site of disease. This is particularly important for evaluating medications that could potentially mitigate or even reverse cortical porosity (and potentially hip fractures) in these patients [38]. As a result, further studies are needed in both animal models and humans to assess the value of the PI for prospectively monitoring disease progression.

In the current study, UTE-MRI was able to detect differences between normal animals and animals with CKD. For example, Cy/+ rats had a higher PI at the distal tibia than their normal counterparts at 30 weeks of age. Though Cy/+ rats did not have a higher PI at the proximal femur than the normal animals at 35 weeks of age (though a trend was present), these results were correlated with Pore% derived from microCT imaging ($\rho = 0.929$). However, there was no correlation between PI and femoral neck mechanical properties (unlike prior studies that did demonstrate a significant relationship [39,40]).

In addition, UTE-MRI failed to detect the progression of cortical porosity observed with microCT imaging at the distal tibia. Although the exact cause is unclear, one potential explanation may be related to signal heterogeneity within the MRI VOIs. The PI is derived from proton signals that exist beyond the detection of high-resolution CT imaging, and the lower spatial resolution of MRI makes it much more susceptible to partial volume effects. As a result, the inclusion of proton signals from the adjacent periosteal and endocortical soft tissues may have decreased the cortical bone signal-to-noise ratio, thereby decreasing the sensitivity of the PI to detect smaller changes in cortical porosity. In addition, prior studies have demonstrated that higher magnetic field strengths limit the ability of T2* to discriminate between bound and pore water compartments due to increased susceptibility [41].

This study was the first to examine the longitudinal relationship between microCT imaging and UTE-MRI in CKD, but there were important limitations. The early deaths of several CKD animals limited the sample size of animals at 35 weeks of age. In addition, though the VOI was defined in a similar manner between timepoints, the lack of image registration may have added variability to the analysis over time. This study also lacked information other relevant disease parameters (such as histological bone turnover, serum turnover markers, and serum markers of kidney function) known to play a role in bone quality in chronic kidney disease [42]. Finally, the Bruker method of scanning and reconstruction does not correct for gradient imperfections in the magnetic field [43,44], which may have reduced the ability to discriminate between bound and pore water compartments in this study.

Finally, this was the first study to evaluate the porosity index using a high (9.4 T) magnetic field strength. Though this field strength provides a strong gradient necessary for high spatial resolution in a rodent model, higher field strengths are suboptimal for distinguishing between bound and pore water compartments due to increasing susceptibility at higher field strengths [41]. Despite the inherent tradeoffs between spatial resolution and increasing susceptibility, the differences at the distal tibia (and possibly even the proximal femur) along with the correlation between PI and Pore% at the proximal femur are especially encouraging. These results are promising and suggest that the more clinically relevant field strengths will better detect changes in porosity that occur in the setting of chronic kidney disease.

5. Conclusions

The current data demonstrate a complex relationship between cortical bone MR imaging and high-resolution CT imaging in animals with CKD. Given the various limitations of each imaging modality, a multimodality approach to diagnosing and monitoring bone disease may be needed. Future studies examining the relationship between dual energy x-ray absorptiometry (DEXA), HR-pQCT, and UTE-MRI may be helpful for exploring the optimal approach to diagnosing and managing CKD-related bone disease. Although more data are still needed, these results indicate that UTE-MRI may have value for evaluating the progression of bone disease in CKD, especially given the lack of ionizing radiation and its ability to evaluate the proximal femur.

Acknowledgments

This work was supported by the RSNA Research & Education Foundation (075717–00002B, CLN). The content is solely the responsibility of the authors and does not represent the official views of the RSNA R&E Foundation. This work was also supported by a United States (U.S.) Department of Veterans Affairs Merit Grant (BX003025, MRA). The contents do not represent the views of the U.S. Department of Veterans Affairs or the United States Government.

Data availability

Data will be made available on request.

References

[1]. Levin A, Bakris GL, Molitch M, Smulders M, Tian J, Williams LA, Andress DL, Prevalence of abnormal serum vitamin D, PTH, calcium, and phosphorus in patients with chronic kidney disease: results of the study to evaluate early kidney disease, Kidney Int. 71 (2007) 31–38. [PubMed: 17091124]

[2]. KDIGO, Clinical practice guidelines for the management of CKD–MBD, Kidney Int. 76 (2009) S1–S130.

[3]. Alem AM, Sherrard DJ, Gillen DL, Weiss NS, Beresford SA, Heckbert SR, Wong C, Stehman-Breen C, Increased risk of hip fracture among patients with end-stage renal disease, Kidney Int. 58 (2000) 396–399. [PubMed: 10886587]

[4]. Dooley AC, Weiss NS, Kestenbaum B, Increased risk of hip fracture among men with CKD, Am. J. Kidney Dis. 51 (2008) 38–44. [PubMed: 18155531]

[5]. Fried LF, Biggs ML, Shlipak MG, Seliger S, Kestenbaum B, Stehman-Breen C, Sarnak M, Siscovick D, Harris T, Cauley J, Newman AB, Robbins J, Association of kidney function with incident hip fracture in older adults, J. Am. Soc. Nephrol. 18 (2007) 282–286. [PubMed: 17167115]

[6]. Nickolas TL, McMahon DJ, Shane E, Relationship between moderate to severe kidney disease and hip fracture in the United States, J. Am. Soc. Nephrol. 17 (2006) 3223–3232. [PubMed: 17005938]

[7]. Nitsch D, Mylne A, Roderick PJ, Smeeth L, Hubbard R, Fletcher A, Chronic kidney disease and hip-fracture-related mortality in older people in the UK, Nephrol. Dial. Transplant. 24 (2008) 1539–1544. [PubMed: 19075194]

[8]. Mittalhenkle A, Gillen DL, Stehman-Breen CO, Increased risk of mortality associated with hip fracture in the dialysis population, Am. J. Kidney Dis. 44 (2004) 672–679. [PubMed: 15384018]

[9]. Nickolas TL, Leonard MB, Shane E, Chronic kidney disease and bone fracture: a growing concern, Kidney Int. 74 (2008) 721–731. [PubMed: 18563052]

[10]. Ott SM, Bone strength: more than just bone density, Kidney Int. 89 (2016) 16–19. [PubMed: 26759040]

[11]. KDIGO, Clinical practice guideline update for the diagnosis, evaluation, prevention, and treatment of chronic kidney disease–mineral and bone disorder (CKD-MBD), Kidney Int. Suppl. 7 (1) (2017).

[12]. Evenepoel P, Cunningham J, Ferrari S, Haarhaus M, Javaid MK, Lafage-Proust MH, Prieto-Alhambra D, Torres PU, Cannata-Andia J, European Renal Osteodystrophy workgroup, an intitiative of the CKD-MBD working group of the ERA-EDTA and the committee of Scientific Advisors and National Societies of the IOF, European consensus statement on the diagnosis and management of osteoporosis in chronic kidney disease stages G4-G5D, Nephrol. Dial. Transplant. 36 (1) (2021) 42–59. [PubMed: 33098421]

[13]. Yenchek RH, Ix JH, Shlipak MG, Bauer DC, Rianon NJ, Kritchevsky SB, Harris TB, Newman AB, Cauley JA, Fried LF, Bone mineral density and fracture risk in older individuals with CKD, Clin. J. Am. Soc. Nephrol. 7 (2012) 1130–1136.

[14]. West SL, Lok CE, Langsetmo L, Cheung AM, Szabo E, Pearce D, Fusaro M, Wald R, Weinstein J, Jamal SA, Bone mineral density predicts fractures in chronic kidney disease, J. Bone Miner. Res. 30 (2015) 913–919. [PubMed: 25400209]

[15]. Jassal SK, von Muhlen D, Barrett-Connor E, Measures of renal function, BMD, bone loss, and osteoporotic fracture in older adults: the Rancho Bernardo study, J. Bone Miner. Res. 22 (2007) 203–210. [PubMed: 17059370]

[16]. Iimori S, Mori Y, AkitaW Kuyama T., Takada S, Asai T, Kuwahara M, Sasaki S, Tsukamoto Y, Diagnostic usefulness of bone mineral density and biochemical markers of bone turnover in predicting fracture in CKD stage 5D patients—a single-center cohort study, Nephrol. Dial. Transplant. 27 (2012) 345–351. [PubMed: 21652550]

[17]. Nickolas TL, Stein E, Cohen A, Thomas V, Staron RB, McMahon DJ, Leonard MB, Shane E, Bone mass and microarchitecture in CKD patients with fracture, J. Am. Soc. Nephrol. 21 (2010) 1371–1380. [PubMed: 20395370]

[18]. McNerncy EMB, Buening DT, Aref MW, Chen NX, Moe SM, Allen MR, Time course of rapid bone loss and cortical porosity formation observed by longitudinal microCT in a rat model of CKD, Bone 125 (2019) 16–24. [PubMed: 31059864]

[19]. van den Bergh JP, Szulc P, Cheung AM, Bouxsein M, Engelke K, Chapurlat R, The clinical application of high-resolution peripheral computed tomography (HR-pQCT) in adults: state of the art and future directions, Osteoporos. Int. 32 (2021) 1465–1485. [PubMed: 34023944]

[20]. Chen M, Yuan H, Assessment of porosity index of the femoral neck and tibia by 3D ultra-short echo-time MRI, J. Magn. Reson. Imaging 47 (2018) 820–828. [PubMed: 28561910]

[21]. Techawiboonwong A, Song HK, Leonard MB, Wehrli FW, Cortical bone water: in vivo quantification with ultrashort echo-time MR imaging, Radiology 248 (2008) 824–833. [PubMed: 18632530]

[22]. Manhard MK, Horch RA, Gochberg DF, Nyman JS, Does MD, In vivo quantitative MR imaging of bound and pore water in cortical bone, Radiology 277 (2015) 221–229. [PubMed: 26020434]

[23]. Seifert AC, Wehrli FW, Solid-state quantitative ^{1}H and ^{31}P MRI of cortical bone in humans, Curr. Osteoporos. Rep. 14 (2016) 77–86. [PubMed: 27048472]

[24]. Rajapaske CS, Bashoor-Zadeh M, Li C, Sun W, Wright AC, Wehrli FW, Volumetric cortical bone porosity assessment with MR imaging: validation and clinical feasibility, Radiology 276 (2015) 526–535. [PubMed: 26203710]

[25]. Hone AL, Ispiryan M, Padalkar MV, Jones BC, Batzdorf AS, Shetve SS, Pleshko N, Rajapaske CS, MRI-derived bone porosity index correlates to bone composition and mechanical stiffness, Bone Rep. 11 (2019), 100213. [PubMed: 31372372]

[26]. Jerban S, Ma Y, Wan L, Searleman AC, Jang G, Sah RL, Chang EY, Du J, Collagen proton fraction from ultrashort echo time magnetization transfer (UTE-MT) MRI modelling correlates significantly with cortical bone porosity measured with micro-computed tomography (μCT), NMR Biomed. 32 (2) (2019), e4045. [PubMed: 30549338]

[27]. Jerban S, Ma Y, Wong JH, Nazaran A, Searleman A, Wan L, Williams J, Du J, Chang EY, Ultrashort echo time magnetic resonance imaging (UTE-MRI) of cortical bone correlates well with histomorphometric assessment of bone microstructure, Bone 123 (2019) 8–17. [PubMed: 30877070]

[28]. Jerban S, Lu X, Dorthe EW, Alenezi S, Ma Y, Kakos L, Jang H, Sah RL, Chang EY, D'Lima D, Du J, Correlations of cortical bone microstructural and mechanical properties with water proton fractions obtained from ultrashort echo time (UTE) MRI tricomponent T2* model, NMR Biomed. 33 (3) (2020), e4233. [PubMed: 31820518]

[29]. Hong AL, Ispiryan M, Padalkar MV, Jones BC, Batzdorf AS, Shetye SS, Pleshko N, Rajapaske C, MRI-derived bone porosity index correlates to bone composition and mechanical stiffness, Bone Rep 11 (2019), 100213. [PubMed: 31372372]

[30]. Moe SM, Chen NX, Seifert MF, Sinders RM, Duan D, Chen X, Liang Y, Radcliff JS, White KE, Gattone II VH, A rat model of chronic kidney disease-mineral bone disorder, Kidney Int. 75 (2009) 176–184. [PubMed: 18800026]

[31]. Moe SM, Seifert MF, Chen NX, Sinders RM, Chen X, Duan D, Henley C, Martin D, Gattone II VH, R-568 reduces ectopic calcification in a rat model of chronic kidney disease-mineral bone disorder (CKD-MBD), Nephrol. Dial. Transplant. 24 (2009) 2371–2377. [PubMed: 19258382]

[32]. Moe SM, Radcliffe JS, White KE, Gattone II VH, Seifert MF, Chen X, Aldridge B, Chen NX, The pathophysiology of early-stage chronic kidney disease–mineral bone disorder (CKD-MBD) and response to phosphate binders in the rat, J. Bone Miner. Res. 26 (2011) 2672–2681. [PubMed: 21826734]

[33]. Moe SM, Chen NX, Newman CL, Gattone II VH, Organ JM, Chen X, Allen MR, A comparison of calcium to zoledronic acid for improvement of cortical bone in an animal model of CKD, J. Bone Miner. Res. 29 (2014) 902–910. [PubMed: 24038306]

[34]. Vorland CJ, Lachcik PJ, Swallow EA, Metzger CE, Allen MR, Chen NX, Moe SM, Hill Gallant KM, Effect of ovariectomy on the progression of chronic kidney disease—mineral bone disorder (CKD-MBD) in female Cy/+ rats, Sci. Rep. 9 (2019) 7936. [PubMed: 31138895]

[35]. Jones BC, Jia S, Lee H, Feng A, Shetye SS, Batzdorf A, Shapira N, Noel PB, Pleshko N, Rajapaske CS, MRI-derived porosity index is associated with whole-bone stiffness and mineral density in human cadaveric femora, Bone 143 (2021), 115774. [PubMed: 33271401]

[36]. Xiong Y, He T, Wang Y, Liu WV, Hu S, Zhang Y, Wen D, Hou B, Li Y, Zhang P, Liu J, He F, Li X, CKD stages, bone metabolism markers, and cortical porosity index: associations and mediation effect analysis, Front. Endocrinol. (Lausanne) 12 (2021), 775066.

[37]. Metzger CE, Newman CL, Tippen SP, Golemme NT, Chen NX, Moe SM, Allen MR, Cortical porosity occurs at varying degrees throughout the skeleton in rats with chronic kidney disease, Bone Rep. 15 (2022), 101612.

[38]. Swallow EA, Metzger CE, Newman CL, Chen NX, Moe SM, Allen MR, Cortical porosity development and progression is mitigated after etelcalcetide treatment in an animal model of chronic kidney disease, Bone 157 (2022), 116340. [PubMed: 35085840]

[39]. Horch RA, Gochberg DF, Nyman JS, Does MD, Non-invasive predictors of human cortical bone mechanical properties: T2-discriminated 1H NMR compared with high resolution x-ray, PLoS One 6 (2011) 1–5.

[40]. Bae WC, Chen PC, Chung CB, Masuda K, DLima D, Du J, Quantitative ultrashort echo time (UTE) MRI of human cortical bone: correlation with porosity and biomechanical properties, J. Bone Miner. Res. 27 (2012) 848–857. [PubMed: 22190232]

[41]. Seifert AC, Wehrli SL, Wehrli FW, Bi-component T2* analysis of pore and bound water fails at high field strengths, NMR Biomed. 28 (7) (2015) 861–872. [PubMed: 25981785]

[42]. McNerny EMB, Nickolas TL, Bone quality in chronic kidney disease: definitions and diagnostics, Curr. Osteoporor. Rep. 15 (3) (2019) 207–213.

[43]. Manhard MK, Harkins KD, Gochberg DF, Nyman JS, Does MD, 30-second bound and pore water concentration mapping of cortical bone using 2D UTE with optimized half pulses, Magn. Reson. Med. 77 (3) (2019) 945–950.

[44]. Zhao X, Lee H, Song HK, Cheng CC, Wehrli FW, Impact of gradient imperfections on bone water quantification with UTE MRI, Magn. Reson. Med. 84 (4) (2019) 2034–2047.

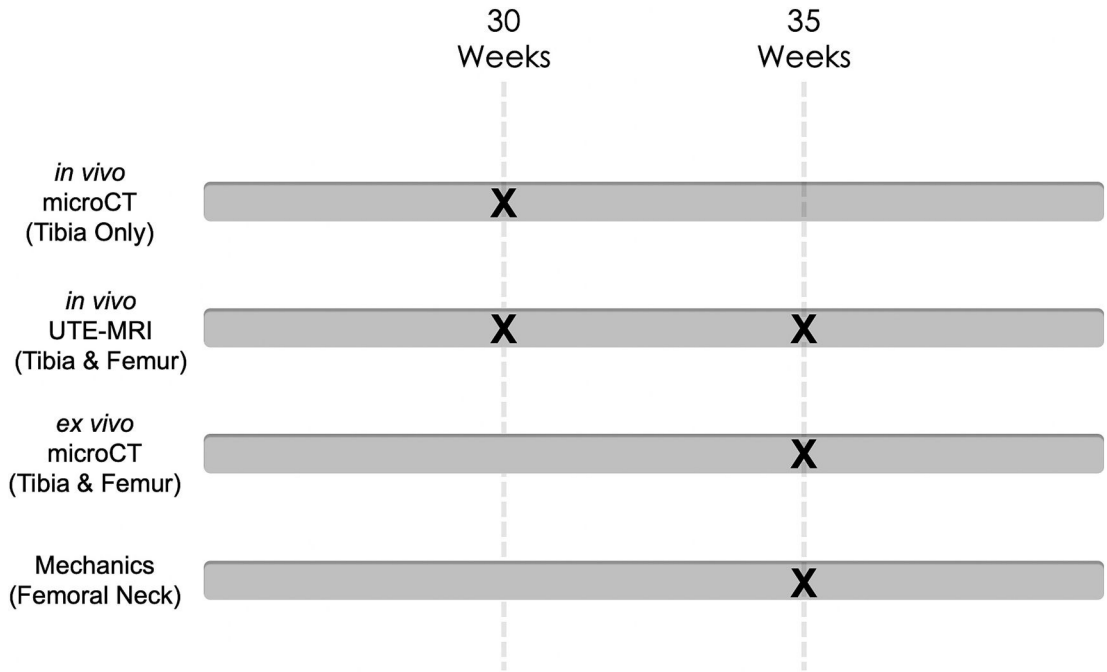

Fig. 1.

Experimental Timeline. Animals underwent *in vivo* microCT imaging of the distal tibiae at 30 weeks. The distal tibiae and proximal femora were imaged at both 30 and 35 weeks of age with *in vivo* UTE-MRI. After euthanasia at 35 weeks, the distal tibiae and proximal femora were imaged using *ex vivo* microCT imaging prior to mechanical testing of the femoral neck.

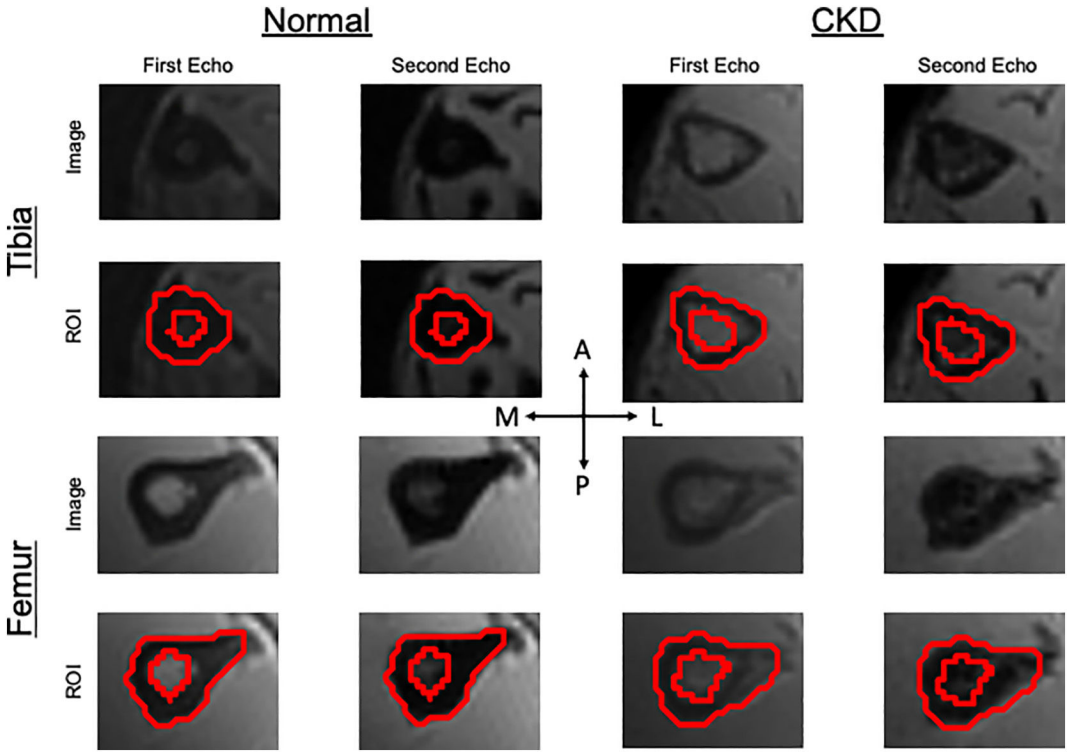

Fig. 2.

UTE-MRI Analysis. Representative images from Cy/+ rats and their normal littermates are depicted. VOIs were obtained from both echoes at the distal tibia and the proximal femur. A = anterior, P = posterior, M = medial, L = lateral.

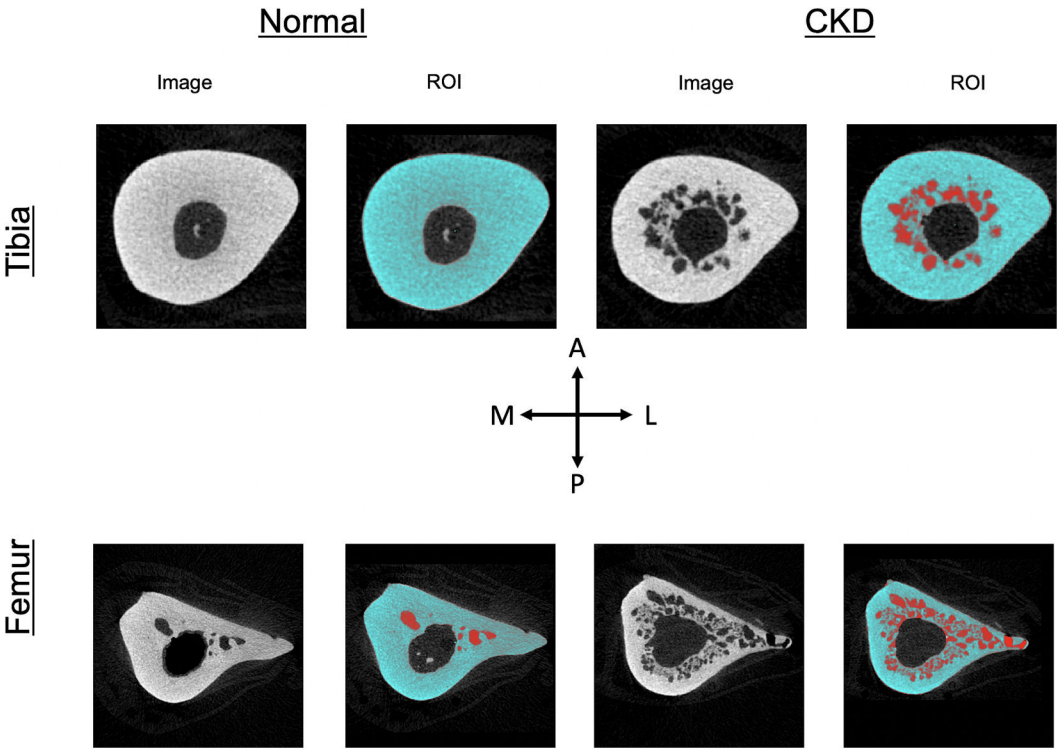

Fig. 3.

microCT Analysis. Representative images from Cy/+ rats and their normal littermates are depicted. VOIs were obtained at the distal tibia and the proximal femur. A = anterior, P = posterior, M = medial, L = lateral.

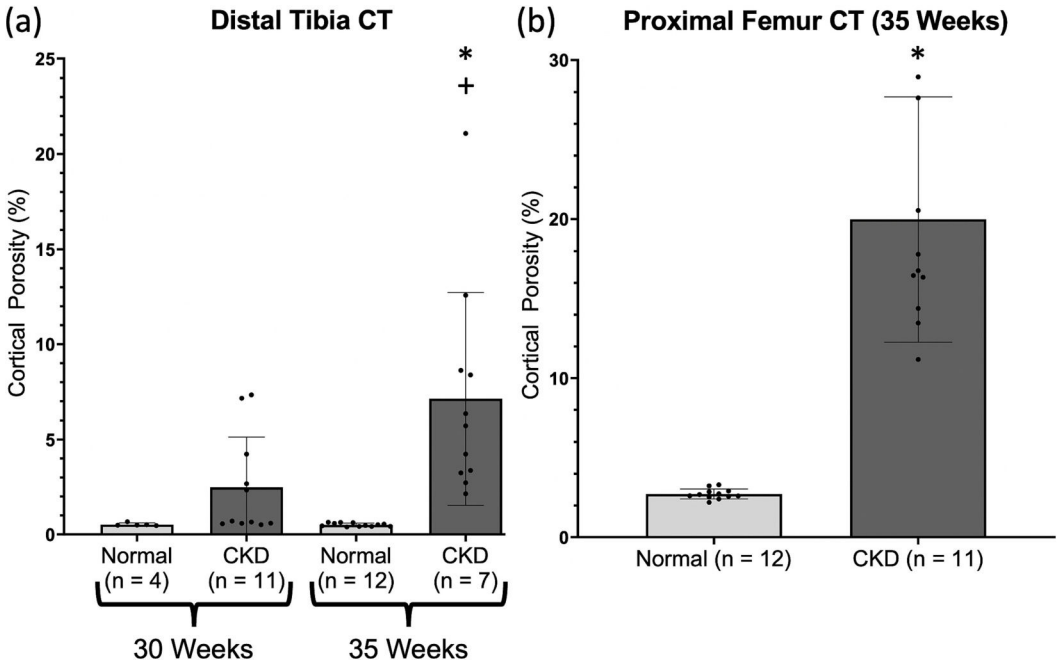

Fig. 4.

microCT Results. (a) Cy/+ rats did not have a greater distal tibia Pore% than the normal rats at 30 weeks (*in vivo*) ($p = 0.009$, ANOVA; $p = 0.751$, Tukey's test), but they did have a greater Pore% at 35 weeks (*ex vivo*) (*p = 0.009, ANOVA; $p < 0.001$, Tukey's test). Pore% in Cy/+ rats increased over the course of the study ($^{+}$p = 0.009, ANOVA; $p = 0.013$, Tukey's test). (b) Cy/+ rats also had a greater *ex vivo* proximal femur Pore% than the normal rats at 35 weeks (*p < 0.001, Welch's *t*-test).

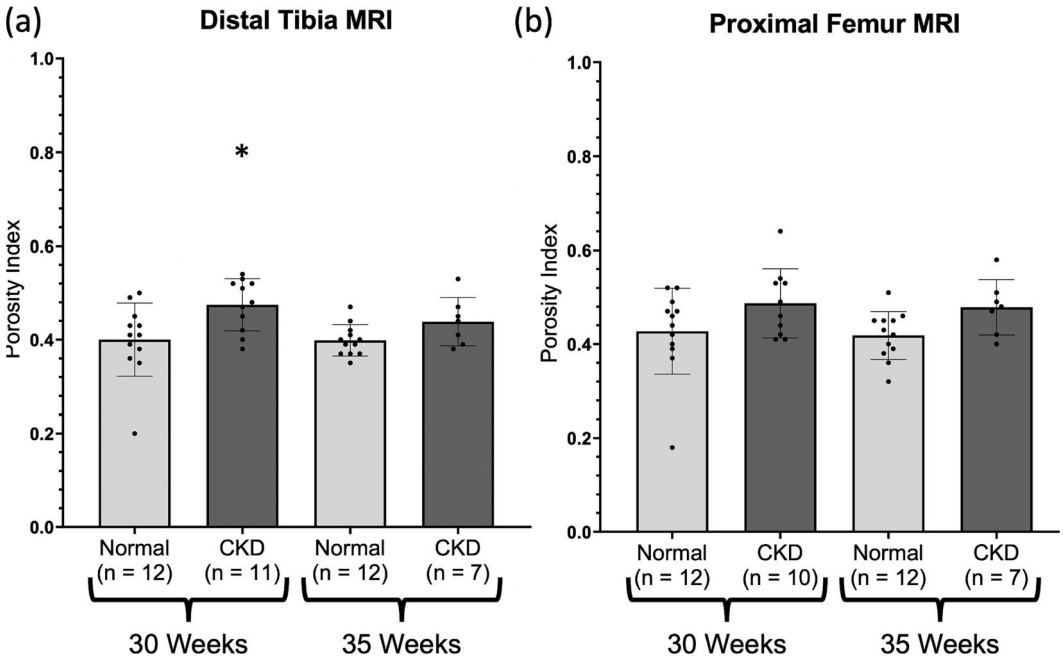

Fig. 5.

UTE-MRI Results. (a) Cy/+ rats had a greater distal tibia PI than the normal rats at 30 weeks (*$p = 0.009$, ANOVA; $p = 0.019$, Tukey's test) but not at 35 weeks ($p = 0.467$, Tukey's test). The distal tibia PI in Cy/+ rats did not increase over the course of the study ($p = 0.575$, Tukey's test). (b) Cy/+ rats did not have a greater proximal femur PI than the normal rats at 30 weeks or at 35 weeks, and the proximal femur PI in Cy/+ rats did not increase over the course of the study ($p = 0.083$, ANOVA).

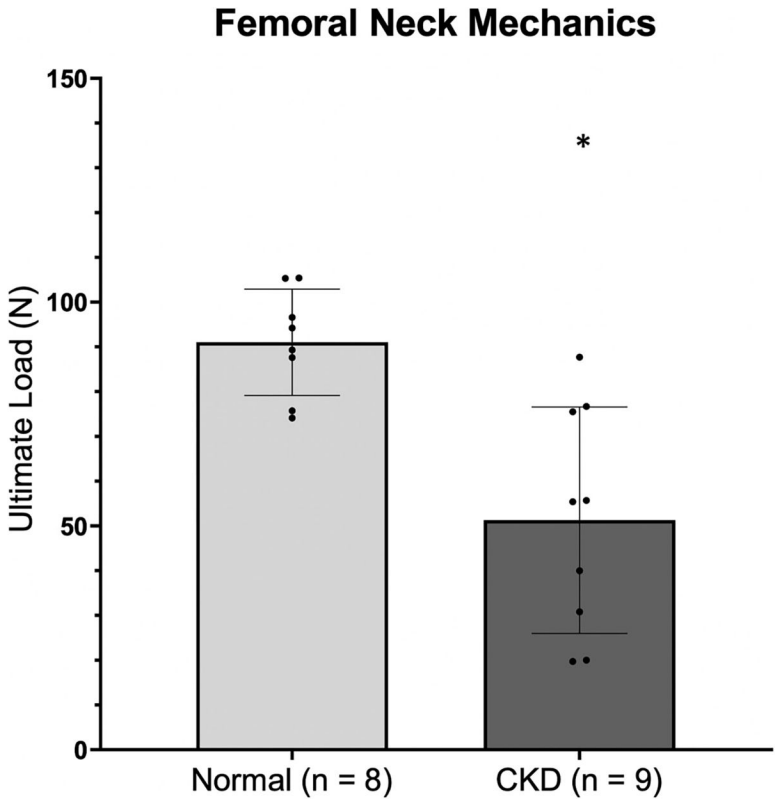

Fig. 6.

Femoral Neck Mechanical Properties. Cy/+ rats had a lower femoral neck ultimate load than normal rats at 35 weeks (*$p = 0.001$, Welch's *t*-test).

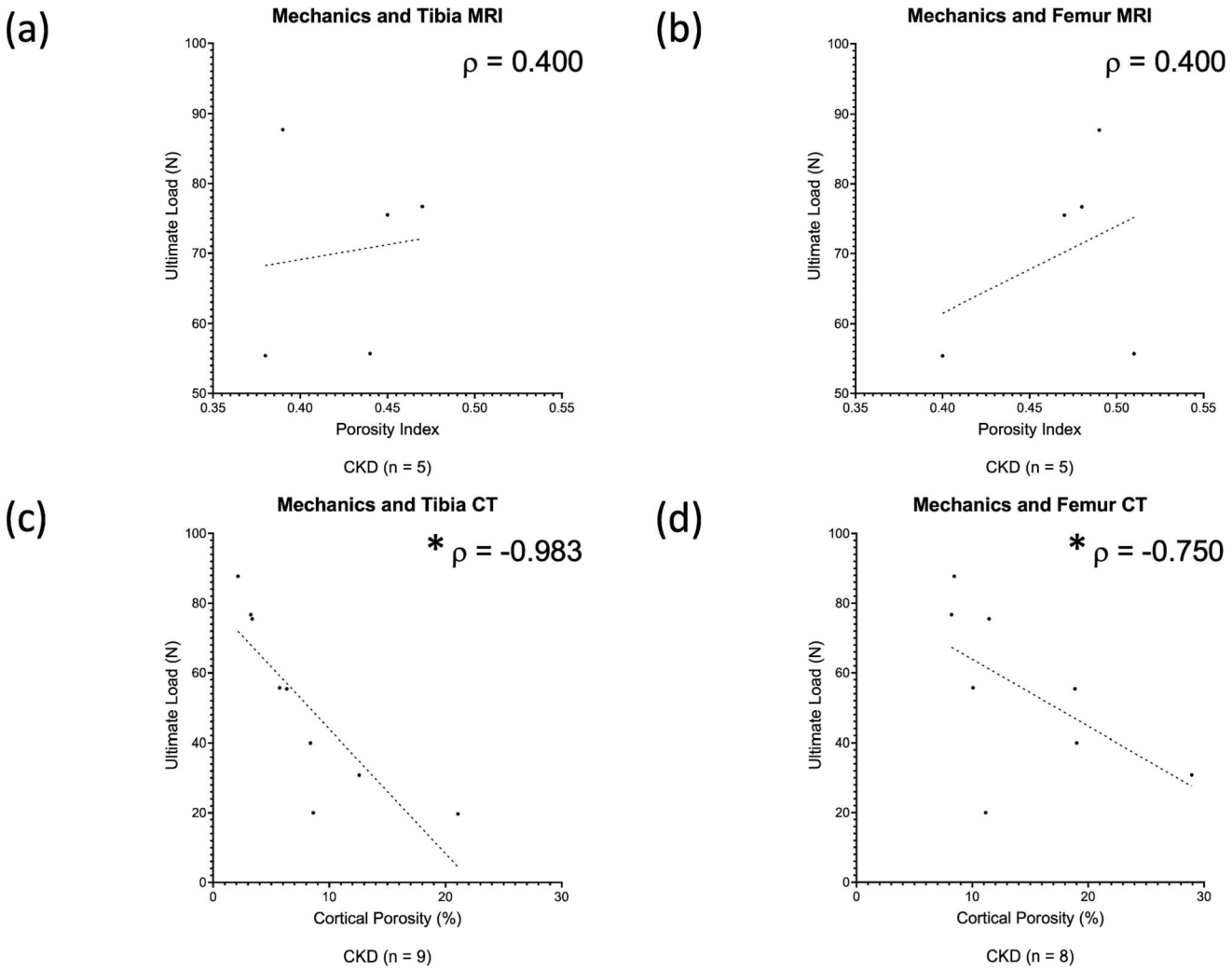

Fig. 7.

Mechanics and Porosity Correlations. (a) There was no correlation between the distal tibia PI and femoral neck ultimate load in CKD animals at 35 weeks ($p = 0.505$) (b) or between the proximal femur PI and femoral neck ultimate load (p = 0.505). (c) However, there was a correlation between the distal tibia Pore% and femoral neck ultimate load (*$p < 0.001$) (d) and between the proximal femur Pore% and femoral neck ultimate load (*$p = 0.020$).

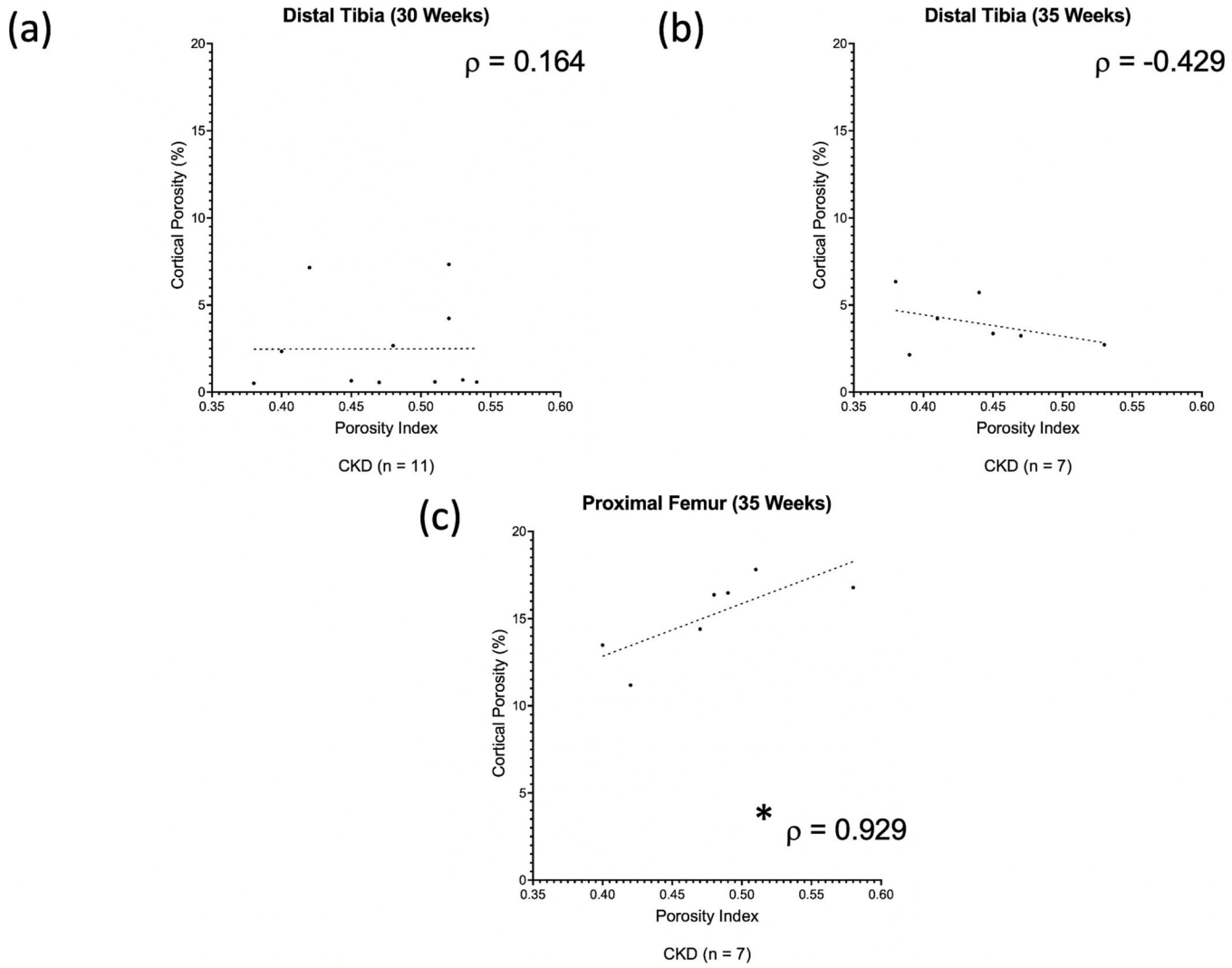

Fig. 8.

microCT and UTE-MRI Correlations. (a) There was no correlation between the distal tibia PI and Pore% in CKD animals at 30 weeks ($p = 0.630$) (b) or at 35 weeks ($p = 0.337$). (c) However, there was a correlation in the proximal femur at 35 weeks (*$p = 0.003$).